p. 15.

(NASA-CR-198814) BOUNDARY-LAYER TRANSITION AND GLOBAL SKIN FRICTION MEASUREMENT WITH AN OIL-FRINGE IMAGING TECHNIQUE (NASA. Ames Research Center) 15 p

N95-30224

Unclas

G3/34 0055499

Boundary-Layer Transition and Global Skin Friction Measurement with an Oil-Fringe Imaging Technique

by

Daryl J. Monson, George G. Mateer and Florian R. Menter
M.S. 229-1, (415)) 604-6255
NASA Ames Research Center
Moffett Field, CA 94035-1000

Paper No. 932550; SAE Aerotech '93; Sept. 27-30, 1993; Costa Mesa, CA

ABSTRACT

A new oil-fringe imaging skin friction (FISF) technique to measure skin friction on wind tunnel models is presented. In the method used to demonstrate the technique, lines of oil are applied on surfaces that connect the intended sets of measurement points, and then a wind tunnel is run so that the oil thins and forms interference fringes that are spaced proportional to local skin friction. After a run the fringe spacings are imaged with a CCD-array digital camera and measured on a computer. Skin friction and transition measurements on a two-dimensional wing are presented and compared with computational predictions.

INTRODUCTION

The importance of data on skin friction in aerodynamic testing has stimulated a continuing effort to develop reliable instrumentation for its measurement. Traditional devices and methods such as floating-element balances, Preston tubes, surface thin-film heat-transfer gauges and pitot-tube surveys combined with the use of a Clauser chart, remain in wide use (1)*. However, all are seriously limited in one or more aspects. For example, they may require permanent installation, be delicate, complex and tedious to use, measure skin friction only indirectly, be applicable to a limited range of flows or be intrusive to the flow.

A more recently-developed method, the laser interferometer skin-friction (LISF) technique, overcomes many of the limitations of the traditional methods. In that method, the thinning due to surface shear of an oil film placed on the test surface is monitored by a laser beam-photodiode interferometer and related to the local skin friction using lubrication theory. The technique provides a direct nonintrusive measurement of skin friction that is relatively simple to use and may be applied in a wide variety of complex flows. Several versions of the method have been developed by Tanner (2), Monson (3), Westphal et al.(4), Kim and Settles (5) and Seto and Hornung (6). In spite of its many advantages, the method still has some limitations. It is sensitive to possible dust contamination, tunnel vibration, model movement and oil evaporation, and it is slow and tedious to use since only one measurement can be made each run. Also, it either requires tunnel optical access for the laser beam during a run (2-5), or permanent installation of a plug in the test body (6).

Tanner and Blows (7) also developed an earlier photographic version of the LISF method. In that method, the interference fringes that formed due to shear on an oil droplet placed on a glass insert in the wind tunnel wall were photographed during a run using He-Ne laser illumination. The fringe spacing measured from the photograph was related to local skin friction using lubrication theory, as in the other LISF methods. The technique had many limitations. It was neither convenient nor accurate since it required a glass insert in the tunnel wall, manual fringe measurements from photographs and crude estimates of "effective" tunnel run time. Thus it was eventually supplanted by the more convenient and accurate photodiode LISF method.

In this paper, a new and innovative testing technique to measure boundary-layer (b.l.) transition and global skin friction on wind tunnel test bodies is presented. This fringe-imaging skin friction (FISF) method is a modern extension and improvement on Tanner and Blows (7) original photographic LISF technique. The new method is accurate and convenient to use, and it overcomes most of the disadvantages of previous LISF methods. For example, it doesn't require either a glass insert or a permanent installation in the test body, but may be used on any solid surface. Also, it is insensitive to tunnel vibration, model movement, oil evaporation and moderate dust contamination. Furthermore, fringe imaging is carried out after a run with nonlaser light, so tunnel optical access during a run is not required. Finally, the method can provide complete (i.e., global) skin friction distributions on a test body in one run by using multiple oil drops or lines, and it can clearly reveal the location of b.l. transition if it occurs.

DESCRIPTION OF FISF METHOD

THEORY - The theoretical basis of the FISF method is illustrated in Figure 1. If a drop or line of oil is placed on a specularly-reflecting wind tunnel surface before a run and then

*. Numbers in parentheses designate references at the end of the paper.

subjected to surface shear τ during a run, it will flow downstream forming an inclined surface with zero thickness at the leading edge that decreases in slope with time t. From lubrication theory (8), the oil-air interface thickness $y_i(s, t)$ in the local flow direction s in the general case of varying $\tau(s)$ and $v_o(T(t))$ is

$$y_i(s,t) = \left(\frac{\frac{\rho_o}{\sqrt{\tau(s)}} \int_0^s \frac{ds}{\sqrt{\tau(s)}}}{\int_0^t \frac{dt}{v_o(T(t))}} \right) \quad (1)$$

Note that if $\tau(s)$ is respectively increasing, decreasing or constant, the corresponding surface is convex, concave or straight. Expansion of $\tau(s)$ in a Taylor series in terms of its value at the origin gives

$$\tau(s) = \tau(0) + \tau'(0)\, s + \ldots \equiv \tau(0) \left[1 + \tau'(0) \left(\frac{s}{\tau(0)} \right) \right] \quad (2)$$

In small regions near the origin,

$$\tau'(0) \left(\frac{s}{\tau(0)} \right) \ll 1 \quad (3)$$

so that $\tau(s) \equiv \tau(0)$. (The practical implications of this restriction will be discussed later.) If $t = t_{run}$ and the average oil viscosity is defined as

$$v_{o,ave}^{-1} = \frac{1}{t_{run}} \int_0^{t_{run}} \frac{dt}{v_o(T(t))} \quad (4)$$

then EQ (1) becomes

$$y_i(s, t_{run}) \equiv \rho_o v_{o,ave} \left[\frac{s}{\tau(0)\, t_{run}} \right] \quad (5)$$

Differentiating EQ (5), the local skin friction at any point in the flow is

$$\tau_{local} \equiv \frac{\left[\frac{\rho_o v_{o,ave}}{t_{run}} \right]}{\left[(\Delta y_i / \Delta s)_{local} \right]} \quad (6)$$

Optical interferometry is employed as illustrated in Figure 1 to measure the local oil slope $(\Delta y_i/\Delta s)_{local}$ in EQ (6). If a wedge of oil is illuminated after a run by incident monochromatic light, dark (or destructive) interference fringes with spacing Δs_f at the values of y_i shown (for normal incidence) can be observed either by eye or with a camera. In the general case the light is inclined at some angle θ_i in the plane defined by the flow direction and local surface normal, and the observer (i.e., the camera) is looking at the specularly-reflected light at the same angle. Thus, $\Delta s = \Delta s_f = \Delta s_{f,image}/cos\theta_i$ and $\Delta y_i = \lambda/(2n_o cos\theta_r)$ (i.e., the oil thickness change between fringes for arbitrary light refraction angle θ_r). (Note that foreshortening causes the image fringe spacing to be less than or equal to the actual fringe spacing.) If the local skin-friction coefficient is defined as $c_{f,local} = \tau_{local}/q_\infty$, EQ (6) becomes

$$c_{f,local} \equiv \left[\frac{2n (\rho_o v_{o,ave}) \cos\theta_r / \cos\theta_i}{q_\infty \lambda t_{run}} \right] \Delta s_{f,image,local}$$

where the refraction angle of the light within the oil, θ_r, is obtained from

$$\cos\theta_r = \cos\left[a\sin\left(\frac{\sin\theta_i}{n_o} \right) \right] \quad (8)$$

Thus

$$\frac{c_{f,local}}{c_{f,ref}} \equiv \frac{(v_{o,ave} \cos\theta_r / \cos\theta_i)_{local}}{(v_{o,ave} \cos\theta_r / \cos\theta_i)_{ref}} \left[\frac{\Delta s_{f,image,local}}{\Delta s_{f,image,ref}} \right] \quad (9)$$

because the other quantities in EQ (7) are constants that cancel out. If θ_i is moderately small or is held nearly constant everywhere, the *cos* terms in EQ (9) also approximately cancel out. If in addition the temperature of the test surface is either nearly constant or varies with time uniformly, $v_{o,ave}$ is nearly constant everywhere and will approximately cancel out. Then EQ (9) may be simplified to

$$\frac{c_{f,local}}{c_{f,ref}} \equiv \frac{\Delta s_{f,image,local}}{\Delta s_{f,image,ref}} \quad (10)$$

Equations (9) or (10) form the basis of the FISF method. The fringe spacing distributions (in the local flow direction) after a run are imaged and then measured on all applied oil lines on the test surface to obtain normalized c_f.

To get absolute values of c_f, $c_{f,ref}$ must be determined. (Note that this needs to be done at only one position on the test body.) There are three ways of doing this: First, it can be measured at the reference point by other independent methods such as LISF or with a Preston tube. This is probably the preferred method. Second, the constants in EQ (7) can be evaluated directly at the reference position, which is the most elegant solution since then the FISF method will stand alone. However, this method is complicated by the fact that the entire history of q_∞ and $v_{o,ave}$ must be accurately known and integrated for the entire run, including tunnel start-up and shutdown times. (This requirement is more stringent than the requirements for the LISF method, which only utilizes a *segment* of the oil-flow time record in the middle of a run when flow conditions are constant.) Third, it can be predicted by a reliable CFD code. The last method is utilized in this paper.

TEST SURFACE - Typical wind-tunnel test surfaces do not produce enough fringe visibility to successfully implement the FISF method, so special surface preparations are normally required. Acceptable surfaces include glass with a reflection-enhancing chromium layer (7) or highly-polished stainless steel (8). Unfortunately, this excludes many types of wind tunnel models, so a new kind of surface preparation has been developed in this study that is applicable to any surface. The first step is to spray the model with flat-black enamel or lacquer. (If sensors or pressure taps on the model must be protected from paint, it can be pre-covered with regular wet-

sive Monocote* using detergent or soapy water so that air bles may be forced out.) Then 2 mil pressure-sensitive (i.e., lf-adhesive) Mylar sheet# is applied to the painted surface sing detergent. (Black Monocote by itself, which is a clear plastic over black paint, also produces visible fringes, but their quality isn't as good as fringes produced by the described surface.) During testing, care should be taken to avoid scratching the mylar surface as that will degrade fringe visibility. If scratches do build up with extended use, the surface should be re-covered periodically.

OIL - Dow DC-200 oil+ has been used to date in the FISF method, which is the same oil that has been used for all previous applications of the LISF method (3). It has desirable properties such as very low vapor pressure and high transparency, and it is available in a wide range of viscosities. This study used 50, 100 and 200 cs viscosity oil, but other studies may find viscosities as low as 10 cs or as high as 1,000 cs useful. (Lower viscosities evaporate too readily and higher viscosities accumulate persistent surface waves.) The choice of oil viscosity is based on experience, and depends both on local shear levels and available tunnel run times. The oil has a well-defined viscosity-temperature variation for use in EQ (4), namely

$$\frac{\upsilon_o(T(t))}{\upsilon_o(T_{ref})} = \exp\{-S[T(t) - T_{ref}]\} \qquad (11)$$

where the constants S and $\upsilon_o(T_{ref})$ are determined by calibration$. (Actually, in this paper EQ (11) was not required since EQ (10) was applied where $c_{f,ref}$ was obtained from CFD solutions.)

To implement the FISF method, a line (or drop) of oil is applied on the test surface with its leading edge approximately along the intended set of measurement points. (If desired, any number of drops or lines may be applied to any number of surfaces, as long as they won't flow into each other.) One point on one line is chosen as the reference position for use in EQ's (9) or (10). The lines do not need to be either straight or normal to the local flow direction (although inclination angles beyond 45° from perpendicular make fringe-spacing measurements sensitive to small errors in knowing the local flow direction). A sloped test surface can cause a problem for the method if gravity causes the applied oil to flow "upstream" before the tunnel is started. This problem can usually be avoided by tilting the surface such that gravity pre-thins the oil in the "downstream" direction, and then correctly positioning the model just before a run. The oil may be applied by any number of methods. In this study, a thin plastic drafting triangle was used. (A commercial "paint-striping" tool and eye dropper were also successfully used for some runs.) The oil was put on the long edge of the triangle by an eye dropper and allowed to even out by gravity. Then, one end of the triangle was touched to the surface against a positioning guide and the oil was applied by "rolling" the triangle edge along the intended measurement line.

FRINGE IMAGING - The fringes are imaged after a run. This requires either post-run tunnel optical access, or the test model may be removed from the tunnel. (It was observed that the "frozen" fringes retain good quality for about an hour if protected from dust and moisture.) A suitable light source and a camera are required to perform the imaging.

A monochromatic light source (having a coherence length of at least twice the oil thickness of a micron or two at the imaging point) is required to produce "sharp" fringes and avoid "rainbow" overlapping fringes that are ambiguous to measure. A laser is the obvious solution, and Tanner and Blows (7) employed a collimated He-Ne laser in their original work to image a small region of oil drops on a flat glass surface. However, a laser isn't suitable for the curved surfaces of the wing used in the present study. It was necessary to develop an *extended* source of diffuse monochromatic light so that a significant region of fringes could be imaged at one time. A custom "light box" containing two side-by-side Phillips PLC 28-watt compact fluorescent light tubes with an aluminum reflector behind them was constructed. (It was observed that incandescent lights do not have the required coherence length to create good-quality fringes.) The front window measured 7"x7", and consisted of a diffusing white plastic sheet and a green color-separation filter "sandwiched" between outer protective clear plastic layers. The narrow-band green dichroic filter% was centered at 5370 A°. (Other colors may be used, but green was observed to provide the "best" fringe visibility.) Lower-powered commercial versions of this green lamp are also available in various sizes@.

The camera used in this study was a commercial 512x512 pixel CCD-array B&W video camera** equipped with a macro-zoom lens. (Higher-resolution arrays would be desirable.) The test model was a two-dimensional (2-D) wing model (to be described). Fringes were imaged in the tunnel after a run with dry shop air slowly flowing through the test section to minimize post-run water condensation and dust accumulation on the cold model, both of which were observed to degrade fringe quality. (This may not be a problem in some tunnels.) The wing was rotated to a vertical position and the camera and light (mounted on compact stands) were placed downstream side-by-side on the tunnel floor. The camera was kept horizontal and the light box was raised or lowered for each image so that the reflected diffuse light from it completely "backlit" the fringes. The oil fringes were sequentially imaged in approximately 1"x1" overlapping segments as illustrated in Figure 2. The value of θ_i was near zero for all of the images (except very near the highly-curved wing leading edge). An inch ruler was placed in the flow direction at the edge of each image to locate the fringe positions on the wing and to provide fringe scaling. The images were acquired by a computer using

*. Top Flite Corp.
#. Tap Plastics Inc.
+. Dow Corning Corp., Midland, Mich., (517) 496-4000
$. Gascogne Laboratories Inc., Baltimore, MD, (301) 285-8510
%. OCLI, Santa Rosa, CA, (707) 545-6440
@. Edmund Scientific Co., Barrington, NJ, (609) 573-6250
**. Sony Corp. of America, Cypress, CA, (714) 229-4197

a commercial 512x512x8-bit frame grabber*. The digitized images were stored on an optical disc for later image processing.

ERROR ANALYSIS AND LIMITATIONS - The FISF method is susceptible to fewer potential sources of error than is the LISF method (7). Model movement and vibration cause problems for LISF but would have no effect on FISF since the fringes are imaged after a run. Oil evaporation would have no effect on FISF since, if present, it would cause the oil to recede uniformly downstream and not change the slope of the oil. Gravity and pressure gradients would have no effect since it can be shown (7) that the oil which flows to form the fringes in the FISF method is always too thin. Shear gradients would have minimal effect on FISF as long as EQ (3) is satisfied. (Some flow situations where EQ (3) may *not* be satisfied is through separation, re-attachment, transition or shock-wave interaction regions. This issue for transition will be evaluated later in this paper.) Three-dimensional (3-D) flows with locally diverging (or converging) surface skin-friction streamlines must be examined further. Tanner and Blows (7) present the general theory for oil flowing subject to shear with non-parallel surface streamlines. Assume that two adjacent streamlines are separated by n_1 at the first dark oil fringe and n_2 at the last (i.e., second in this paper) downstream fringe. An approximate linearized solution of the general theory will then show that

$$\frac{c_{f,\,local,\,corr}}{c_{f,\,local,\,uncorr}} \cong \frac{1}{2}\left(\frac{3+\frac{n_2}{n_1}}{1+\frac{n_2}{n_1}}\right) \qquad (12)$$

Note that when $n_2 > n_1$ (i.e., diverging streamlines) the correction decreases c_f, when $n_1 = n_2$ there is no correction, and when $n_2 < n_1$ (i.e., converging streamlines) the correction increases c_f. Thus, to minimize measurement errors in 3-D flows, either $\Delta s_{f,image}$ should be chosen small enough so that $n_1 \cong n_2$, or EQ (12) should be applied to correct the data. (This would require a separate conventional oil-flow image of surface streak lines from which n_1 and n_2 could be estimated in the region of interest.)

Based on the previous discussion, it can be concluded that the only significant errors in the FISF method are those that occur from measuring the quantities in EQ (9). First consider the viscosity terms. Most test models either don't change much in temperature or they change temperature uniformly during a run. Therefore the $\nu_{o,ave}$ terms in EQ (9) will in most cases cancel out. Also, EQ (9) is insensitive to the *cos* terms in it if either the values of θ_i are kept small or the variations of θ_i from image to image are kept moderate. (Moderate variations in θ_i have little effect on accuracy because as θ_i is increased, the fringe spacing will increase but the *imaged* fringe spacing will decrease, with the two effects approximately cancelling each other out. For example, to keep the error in computed c_f from EQ (9) to ±1% only requires holding the accuracy of θ_i to ±12°. This is very easy to achieve.) Thus in most cases the only significant errors in the FISF method are those that occur from determining the quantities in EQ (10), namely $\Delta s_{f,image}$, $c_{f,ref}$. Many factors influence the accurate measurement of $\Delta s_{f,image}$. These include the angle of the applied oil line to the local flow direction, the accuracy with which the local flow direction is known, the width and total number of fringes measured, the camera field-of-view and pixel resolution, and the extent of digital image enhancement and smoothing. Some of these factors will be discussed later in the paper. Methods of measuring $c_{f,ref}$ such as LISF are accurate to about ±5% (8). It is expected that evaluating the constants in EQ (7) to get $c_{f,ref}$ will yield close to the same accuracy.

Like the LISF method, the FISF method has some inherent limitations that probably cannot be overcome. Situations which violate EQ (3) have been discussed. Also, the method is sensitive to severe dust and moisture contamination (it destroys the fringes), very high shear levels (surface waves form), very low shear levels (the oil doesn't flow) or high surface temperatures (the oil completely evaporates). These limits are flexible, however, and should be investigated for each individual application.

EXPERIMENT

The FISF method is applied in this study to skin-friction measurements on the top and bottom surfaces of a 2-D supercritical wing model (designated MBB VA-2) tested at a low subsonic speed. The wing has a chord of 20 cm, an aspect ratio of 2, and spans the tunnel between sidewalls (9). The tests were run in the NASA Ames High Reynolds Channel No. 2 (10). It is a blowdown facility using unheated dry air at ambient temperature. Suction panels removed the sidewall boundary layers ahead of the wing to assure flow two-dimensionality. The Mach number was fixed at 0.2. The Reynolds number was varied between 0.7×10^6 and 7×10^6 by changing the tunnel stagnation pressure between 10 and 100 psia, respectively. The wing angle of attack was varied between 0 and 12 degrees. Thermistor sensors on the wing surface recorded the wing temperatures, and revealed considerable (but uniform) model cooling during a run. Tunnel run times between 30 sec and 3 min and oil viscosities of either 50, 100 or 200 cs were selected based on expected run shear levels. For this test, a single line of oil was usually applied at a 45° angle to the flow in a straight line from the wing leading to the trailing edge (although a few runs were made with a line of oil applied in the spanwise direction at various chord positions to verify flow two-dimensionality).

COMPUTATION

For comparison with the FISF experiment, skin friction and b.l. transition were calculated on the MBB VA-2 wing for selected test conditions using a 2-D Navier-Stokes CFD code INS2D (11). The calculations used a 599x121 "C" grid with integration to the wall. The first grid point off the wall was located at $y^+ = 0.5$. A typical CPU time for solution convergence on a Cray YMP computer was 10 min. The turbulence model used was the SST k-ω model of Menter (12), combined with the transition model of Wilcox (13). A detailed evaluation of transition models based on the new c_f data will be performed in the future. The present computations are merely included to demonstrate the good agreement of the data and the numerical

*. Data Translation Inc., Marlboro, MA, (617) 481-3700

s in the laminar and fully-turbulent regions.

SULTS AND DISCUSSION

This section will present the results of applying the FISF method to measure skin friction and transition locations on the MBB VA-2 wing model. First, typical fringe images and the method of measuring fringe spacing from them will be shown. Then, representative c_f and x_t data will be shown and compared with CFD predictions. Finally, future planned improvements and applications of the method will be discussed.

FRINGE IMAGES AND ANALYSIS - Typical fringe images obtained on the model are shown in Figures 2-5. Figure 2(a) illustrates how the oil line was applied on the wing at about 45° and the approximate field-of-view of a single image. About 8 overlapping images were required to record the complete fringe record for a run. Figure 2(b) shows "smooth" laminar-flow fringes on the upper surface near the wing leading edge, with transition just starting near the bottom of the image. (The image is "stretched" horizontally.) Note the large spacing due to high shear near the leading edge. Accurate measurements are difficult there, however, due to the extreme surface curvature. (The dark parts of the image are where no "backlighting" from the light box is present.) Transitional flow fringes which overlap the previous image are shown in Figure 2(c). Notice how irregular they are because of the spanwise variations in transition location in this region. (Transition location is defined in this study as where the fringe spacing, and thereby c_f, first begins suddenly increasing in the laminar region.) Figure 2(d) shows fully-turbulent flow fringes further downstream of the previous image. The fringes are once again "smooth" and gradually decrease in spacing in the flow direction.

Fringes from oil applied in the spanwise direction are shown in Figure 3. Figure 3(a) is from a transitional region, and shows the same fringe "waviness" that was observed in Figure 2(c). Figure 3(b) is in a turbulent region, and shows a constant fringe spacing that is consistent with the flow being 2-D. (The other spanwise images at this chord location all show the same constant fringe spacing.)

Figure 4 shows the oil in a region on the lower wing surface where the method fails. This is a region of low laminar shear combined with an adverse pressure gradient. The "thick" oil from the middle of the applied oil line is "pushed" upstream by the pressure gradient so that the fringes at the leading edge cannot form. Further downstream, the flow is turbulent, the shear is high, and good fringes can once again can be observed. (This problem could possibly be avoided by either pre-thinning or using lower viscosity oil.)

Figure 5 illustrates how the fringe spacings are measured from the fringe images. The top of the figure shows a blowup of a small fringe region with a line indicated in the local flow direction. Because the flow was 2-D, this direction was always along the wing chord. (The image is rotated 90 deg. from the orientation of the original photograph.) The bottom of the figure shows the image intensity plotted along the described line obtained using commercial image-processing software (i.e., PV-WAVE*). The fringe spacing (in pixels) was visually measured from the middle of the first two adjacent dark fringes as shown. The fringe spacing (in inches) was obtained by then determining the pixels/inch from the image of the ruler at the edge of every picture. This process was repeated at about 8 positions per image (and for all 8 images) until a complete data file of fringe spacings (along with their x positions) was created for each run. A reference position was then chosen and EQ (10) applied to compute normalized $(c_{f,local}/c_{f,ref})(x/c)$ for the run. (Note that applying EQ (10) very near the wing leading and trailing edges may result in somewhat low values of c_f because of nonzero and variable θ_i in those regions.)

Recall from the previous error analysis that the measurement of fringe spacing is the only significant source of potential error for *normalized* c_f in the FISF method. Reference to Figure 5 reveals some of the possible sources of error in this measurement. First recall that it is important to accurately know the local flow direction in which to measure the fringe spacing when the oil line is *not* applied normal to that direction (as in the present test). For the present 2-D test the flow direction is accurately known, but this could be an important issue in 3-D tests where the flow direction varies from point-to-point. Also note that the fringes in the top image have vertical striations that produce undesirable fluctuations in the lower image-intensity plot. This makes it difficult to visually identify the middle of the first two dark fringes. The following future improvements could considerably improve fringe-spacing measurement accuracy:

1. Use of a high-resolution CCD-array digital still camera for imaging would enhance image detail and signal-to-noise ratio over the standard television camera used in this study.

2. Digital enhancement and smoothing of both the images and the image intensity plots would allow unambiguous identification of the fringe centers.

3. If multiple fringes are present, the distance between several could be measured and averaged (as long as EQ (3) is satisfied) to "smooth out" the effects of local small disturbances on the fringes. For example, in Figure 5 there appears to be three or four useful fringes. (If desired, one could also choose the center of a light fringe as the downstream fringe to increase the number available.)

4. A zero (or dark level) subtraction as well as a bias (or uniform illumination level) correction to the fringe images in order to correct for pixel-to-pixel gain and offset variations in the camera CCD array could be performed.

SKIN FRICTION COMPARISONS - Some representative c_f distributions obtained using the FISF method on the upper and lower surfaces of the MBB VA-2 wing are compared with theory in Figure 6. For each plot the data were obtained on two separate tunnel runs. (When measuring on the lower surface, the wing was installed inverted in the tunnel to facilitate oil application.) In all cases shown, $c_{f,ref}$ for the data was taken as the theoretical value at x/c = 0.1 (i.e., theory and experiment always agree at that chord location.). Figure 6(a) shows the comparisons at a low Re and α. Here, $c_{f,ref}$ is in the laminar flow region on both surfaces. The data and theory are in remarkably good agreement on both surfaces (with the

*. Precision Visuals Inc., Boulder, Colo., (303) 530-9000

exception of the transition location on the upper surface). Notice that the turbulent region data on the upper surface has a fair amount of scatter. (This is not too surprising since the previously-discussed planned improvements to the fringe-measurement procedure were not yet available for this paper.) Also, note that the c_f values very near the wing leading edge (and possibly trailing edge) may be somewhat low because θ_i there is nonzero, and EQ (9) (which contains the θ_i terms) was not utilized. Finally, the first few points in the transition region may have some error because they fail to satisfy EQ (3) (i.e., the shear changes by up to 20% over one fringe spacing). However, since transitional regions have naturally high scatter in c_f, small measurement errors in that region are probably unimportant.

Figure 6(b) shows the comparisons for a higher Re and α. On the upper surface, transition now occurs very near the leading edge and $c_{f,ref}$ is in the turbulent flow region. On the bottom surface, the reference position has laminar flow, but the data show a "double" transition. This occurs because of spanwise variation in transition location. The 45° applied oil line passes back-and-forth between turbulent and laminar flow in this region. Except for this measured feature, the data and theory are once again in excellent agreement on both surfaces.

TRANSITION LOCATION COMPARISONS - Measured and a few computed transition locations on the MBB VA-2 wing model are compared in Figure 7. (Recall that this location is defined here as x/c where c_f first starts increasing from laminar values. For example, on the upper surface in Figure 6(a) this would be $x_t/c \equiv 0.2$. Most points in Figure 7 are the average of several runs.) The data in Figure 7(a) for the upper surface show that transition quickly moves to near the leading edge for either increasing Re or α. The two predictions agree fairly well with the data. (No data is shown for $\alpha = 4$ deg. at the highest Re because transition was too far forward to accurately measure with the FISF method.) The data in Figure 7(b) for the lower surface show that increasing Re moves transition moderately forward but that increasing α moves it rearward. (This probably occurs because the beginning of the adverse pressure gradient on the bottom moves rearward as α is increased.) For cases as in Figure 6(b) where two transition locations are indicated, the most rearward one was always chosen. The prediction is good at low Re but fairly poor at high Re. No accuracy claims for the present transition model are intended, but these comparisons for transition location demonstrate how the FISF method should be extremely useful in validating any transition model. (Alternately, the data can be used to fix transition location in CFD codes that don't predict transition to assure that the same type of flow is being compared.)

FUTURE DEVELOPMENTS AND APPLICATIONS - The FISF method described in this paper has only recently been developed, and several future improvements to and new applications of it are planned. New data acquisition and reduction procedures that should greatly improve fringe-spacing measurement accuracy (and thereby normalized c_f from EQ (10)) have been discussed. In addition, the method will be extended to measure absolute c_f (i.e., $c_{f,ref}$) by solving for the constants in EQ (7). That method will be evaluated by comparing results from it in a simple 2-D flat plate b.l. flow with $c_{f,ref}$ measurements using other independent methods such as LISF and Preston tubes. Also, the FISF method will be applied in a variety of new situations, including hyperso D, separated, and transonic 2-D shock-wave/b.l. intera flows.

SUMMARY AND CONCLUSIONS

A new technique for measuring skin-friction distributions on wind tunnel models during a single test run has been described and demonstrated. This fringe-imaging skin friction (FISF) technique uses optical interferometry to locally measure the deformation of applied oil lines on the test surfaces. Lubrication theory is then used to infer the local skin friction that caused the oil deformation. The method has been successfully demonstrated in this study for the measurement of both skin friction and transition location on the upper and lower surfaces of a 2-D wing at a subsonic Mach number over a range of angle of attack and Reynolds number. Excellent agreement was obtained with theoretical calculations of skin friction for the wing at two widely-different test conditions using the theory in the laminar regions for reference skin friction. The significant features of the method and conclusions of this study are as follows:

1. The method is easy and robust to use and may be applied to any solid test surface and any type of flow.

2. Fringe imaging is carried out after a run with non-laser light, so optical access during a run is not required.

3. It can provide complete and continuous quantitative skin-friction distributions on any number of test surfaces in a single run. (This is in contrast to most other skin-friction methods which provide only single-point measurements.)

4. It is completely insensitive to model movement, vibration, gravity and pressure gradients, and moderately insensitive to oil evaporation, shear gradients, 3-D flow streamline curvature and divergence, and dust contamination. The only significant sources of error are the accuracies with which fringe spacing and a reference value of skin friction are measured. (A reference value of skin friction is needed at only one point, and may be obtained using other experimental methods, from reliable theory, or may be obtained by solving for constants in the FISF theory itself.)

5. It accurately locates boundary-layer transition if present.

NOMENCLATURE

c	: wing chord
c_f	: skin-friction coefficient
M	: Mach number
n	: index of refraction; also, spacing between adjacent streamlines
q	: dynamic pressure
Re	: Reynolds number based on wing chord
s	: distance in local flow direction measured from oil leading edge
S	: oil viscosity-temperature slope
t	: time
T	: temperature
x	: downstream distance measured from wing leading edge
y	: vertical distance measured from test surface

y^+	: inner variable coordinate normal to the surface
α	: wing angle of attack
Δ	: differential change in quantity
θ	: angle
λ	: light wavelength
ν	: kinematic viscosity
ρ	: density
τ	: skin friction
τ'	: derivative of τ w.r.t. s

Subscripts

ave	: averaged over tunnel run
corr	: corrected for streamline divergence
f	: between adjacent dark fringes
i	: oil-air interface; also, incidence
image	: measured on image
local	: local value
o	: oil
r	: refraction
ref	: reference location or temperature
run	: tunnel run
t	: transition
uncorr	: uncorrected for streamline divergence
∞	: free-stream conditions
1	: first dark fringe
2	: second (or last) measurement fringe

REFERENCES

1. Winter, K. G.: "An Outline of the Techniques for the Measurement of Skin Friction in Turbulent Boundary Layers," *Progress in the Aeronautical Sciences*, Vol. 18, Pergamon Press, Great Britain, 1977, pp. 1-57.

2. Tanner, L. H.,: "A Skin Friction Meter, Using the Viscosity Balance Principle, Suitable for Use with Flat or Curved Metal Surfaces," *Jour. of Physics E: Scientific Instr.*, Vol. 10, No. 3, Mar. 1977, pp. 278-284.

3. Monson, D. J.: "A Nonintrusive Laser Interferometer Method for Measurement of Skin Friction," *Exper. in Fluids*, Vol. 1, No. 1, 1983, pp. 15-22.

4. Westphal, R. V., Bachalo, W. D. and Houser, M. H.: "Improved Skin Friction Meter," NASA TM 88216, Mar. 1986.

5. Kim, K. S. and Settles, G. S.: "Skin-Friction Measurements by Interferometry," *AGARDograph 315*, 1989, pp. 4.1-4.8.

6. Seto, J. and Hornung, H.: "Two-Directional Skin Friction Measurement Utilizing a Compact Internally-Mounted Thin-Liquid-Film Skin Friction Meter," AIAA Paper 93-0180, Reno, NV, Jan. 1993.

7. Tanner, L. H. and Blows, L. G.: "A Study of the Motion of Oil Films on Surfaces in Air Flows, with Application to the Measurement of Skin Friction," *Jour. of Physics E. Scientific Instr.*, Vol. 9, No. 3, Mar. 1976, pp. 194-202.

8. Monson, D. J., Driver, D. M. and Szodruch, J.: "Application of a Laser Interferometer Skin-Friction Meter in Complex Flows," in *Proceedings of the ICIASF*, IEEE Publ. 81CH1712-9, Sept. 1981, pp. 232-243.

9. Mateer, G. G., Seegmiller, H. L., Hand, L. A. and Szodruch, J.: "An Experimental Investigation of a Supercritical Airfoil at Transonic Speeds," NASA TM 103933, July 1992.

10. McDevitt, J. B. and Okuno, A. F.: "Static and Dynamic Pressure Measurements on a NACA 0012 Airfoil in the Ames High Reynolds Number Facility," NASA TP 2485, June 1985.

11. Rogers, S. E. and Kwak, D.: "An Upwind Differencing Scheme for the Time-Accurate Incompressible Navier-Stokes Equations," AIAA Paper 88-2583, Williamsburg, VA, 1988.

12. Menter, F. R.: "Zonal Two Equation k-ω Turbulence Models for Aerodynamic Flows," AIAA Paper 93-2906, Orlando, FL, July 1993.

13. Wilcox, D. W.: "The Remarkable Ability of Turbulence Model Equations to Describe Transition," in *Proceedings of the Fifth Symp. on Numerical and Physical Aspects of Aerodynamic Flows*, Cal. State U., Long Beach, CA, Jan. 1992.

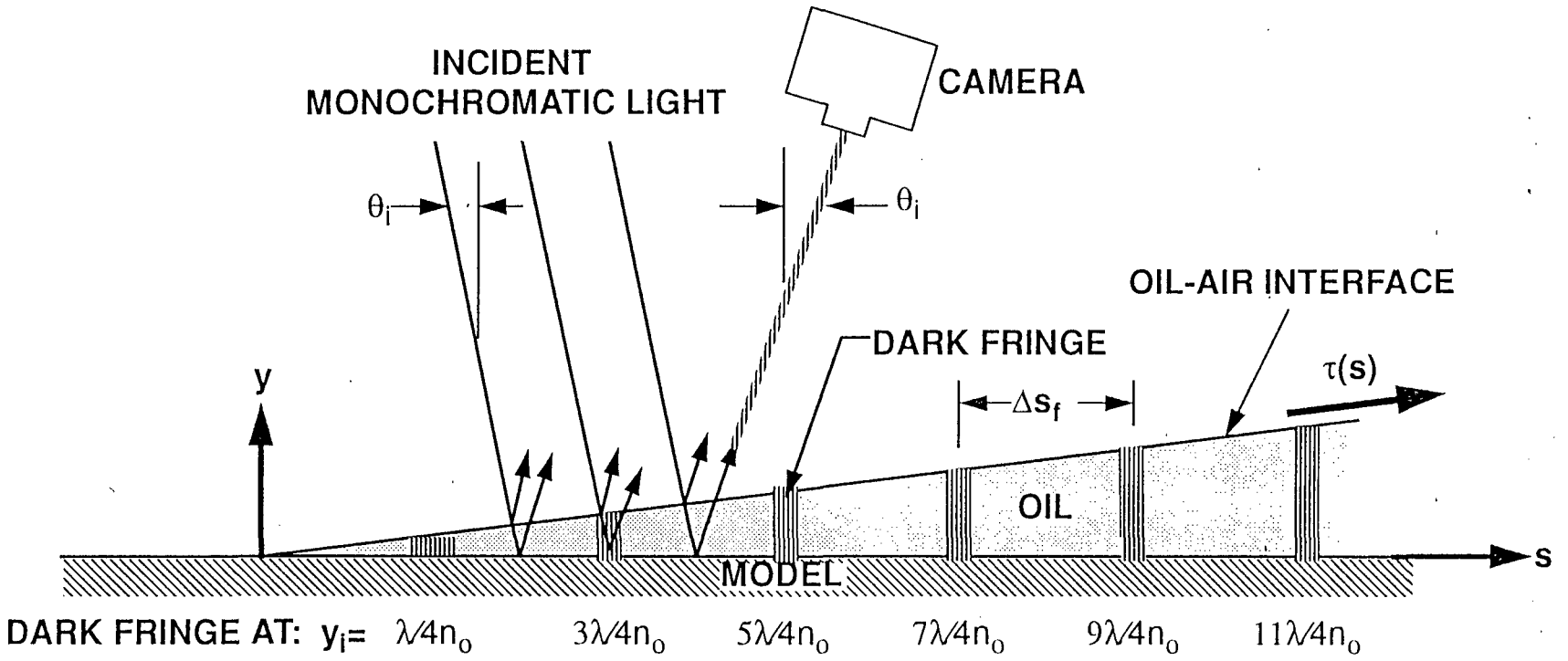

Figure 1. Interference pattern produced by oil film

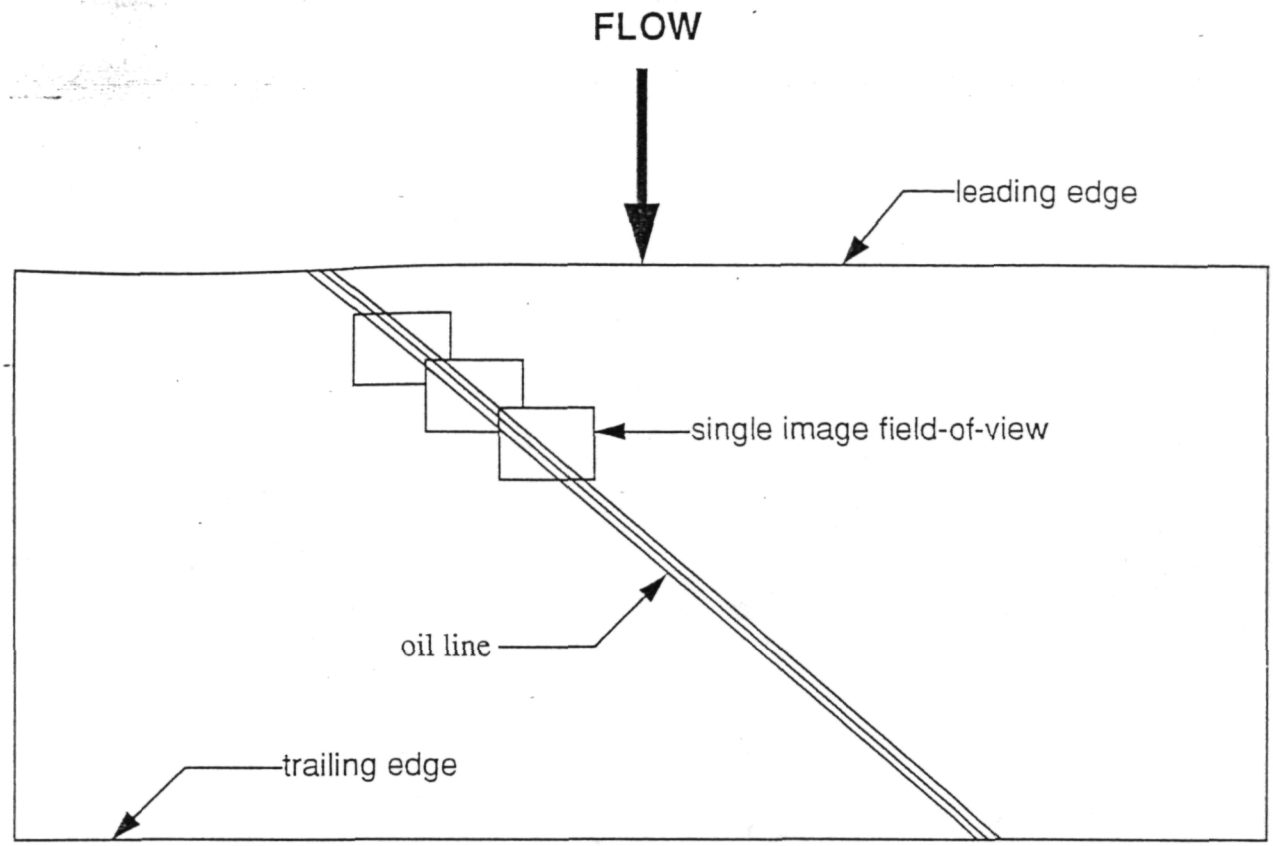

2(a) Planview of MBB VA-2 wing.

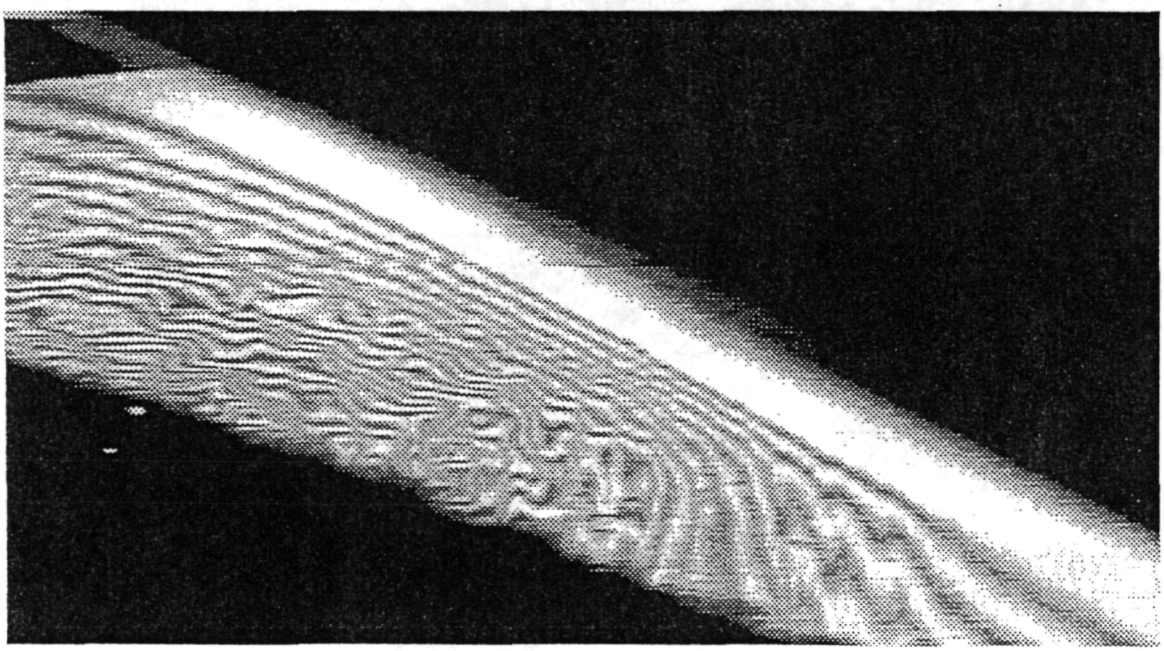

2(b) Laminar flow interference fringes

Figure 2. Fringe-imaging skin friction (FISF) method illustrated

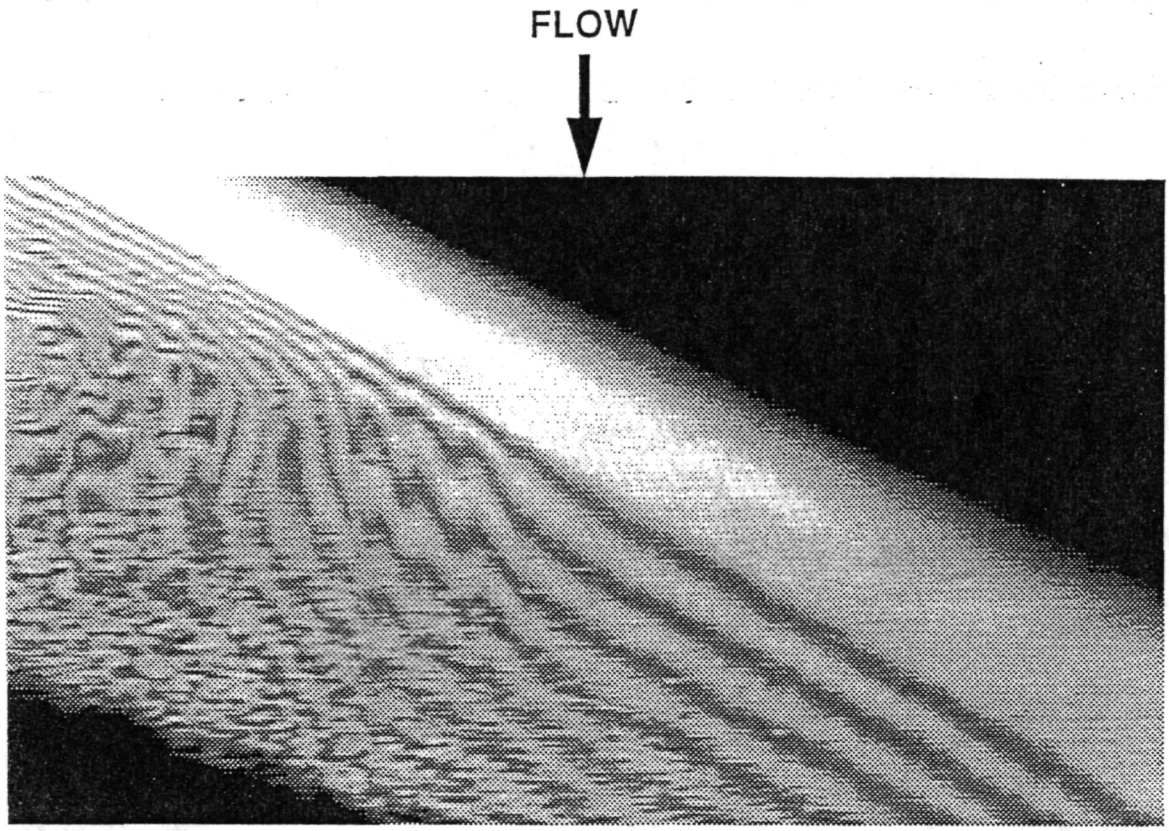

2(c) Transitional flow interference fringes

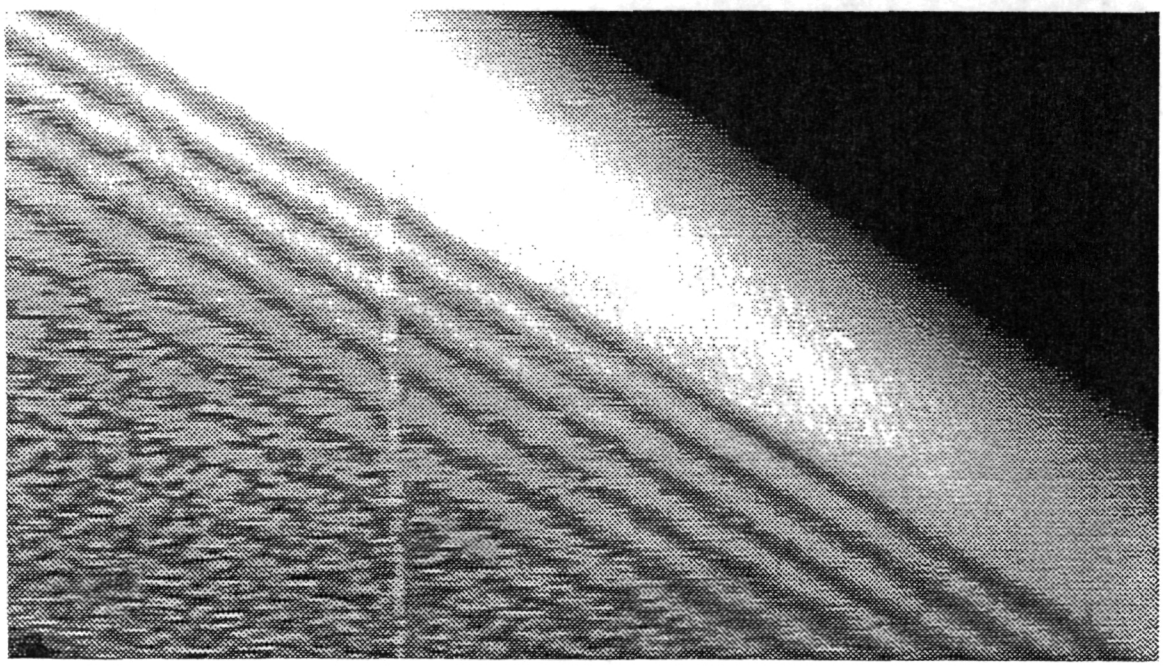

2(d) Turbulent flow interference fringes

Figure 2. Concluded.

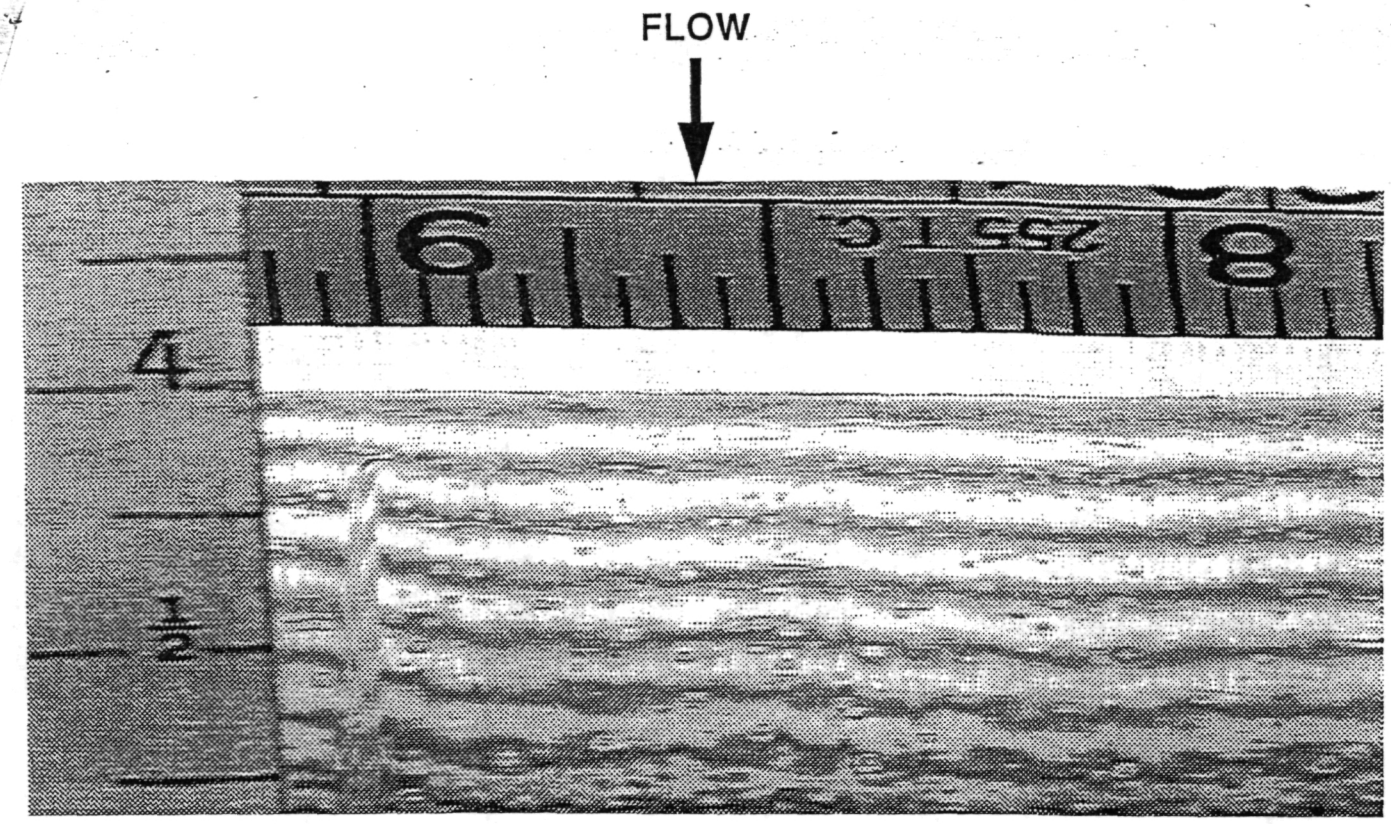

3(a) Transitional flow fringes, x/c=0.51

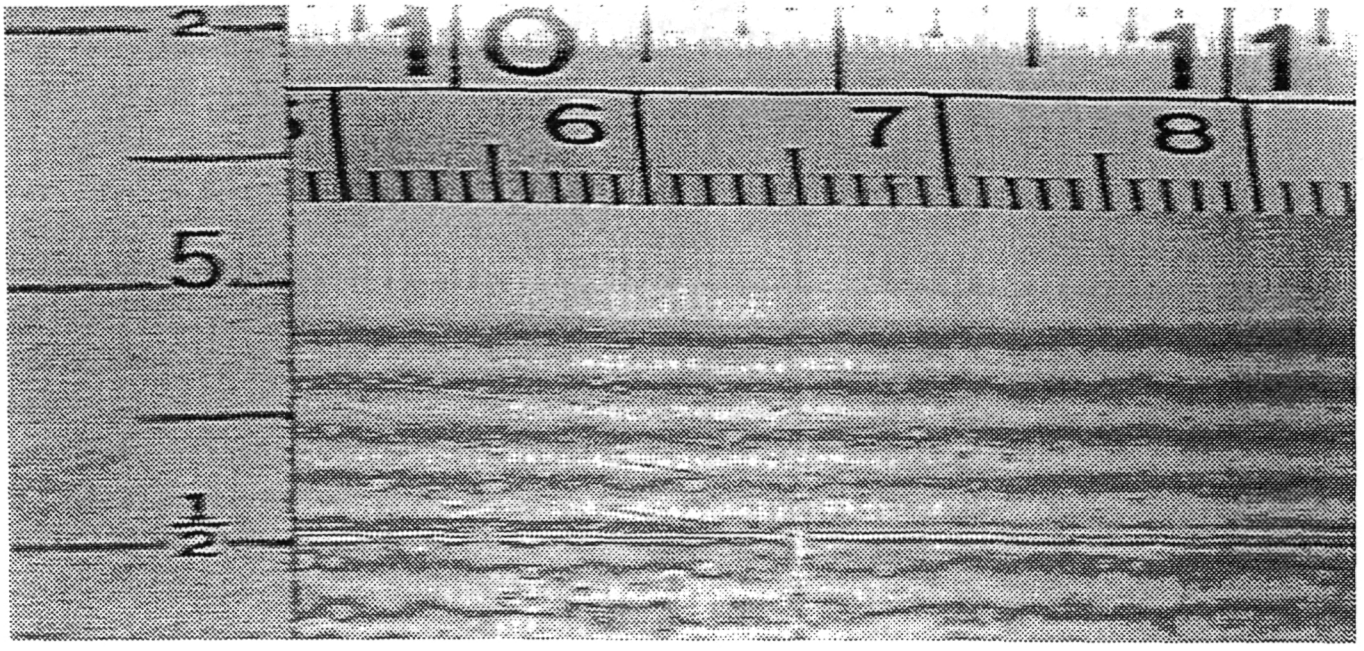

3(b) Turbulent flow fringes, x/c=0.63

Figure 3. Spanwise interference fringes on MBB VA-2 wing upper surface, M_∞=0.2, Re=1x10^6, α=0 deg.

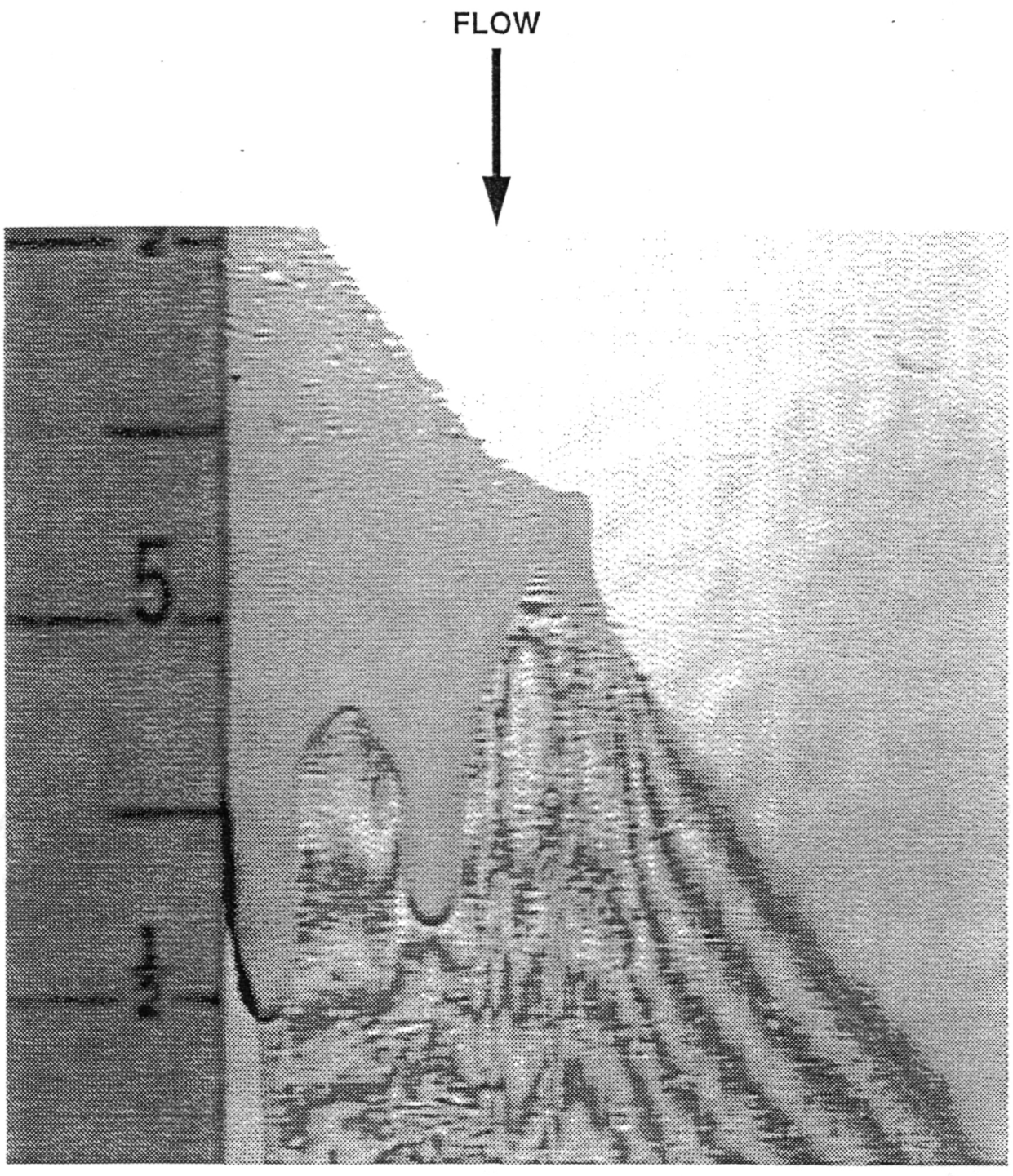

Figure 4. Interference fringes on MBB VA-2 wing lower surface in a region of low laminar shear and adverse pressure gradient,
M_∞=0.2, Re=1x10^6, α=8 deg.

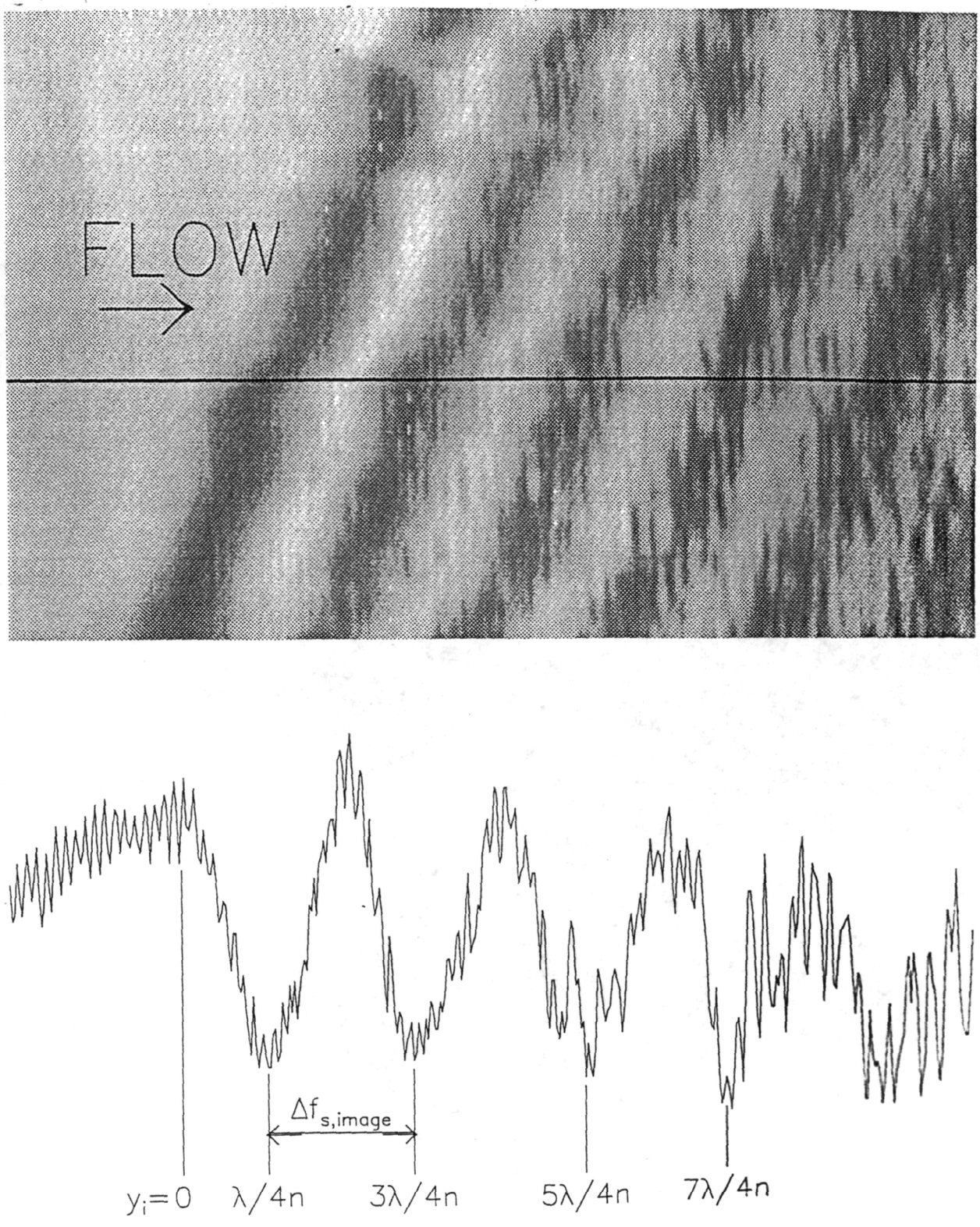

Figure 5. Typical measured oil-fringe intensity variation in flow direction

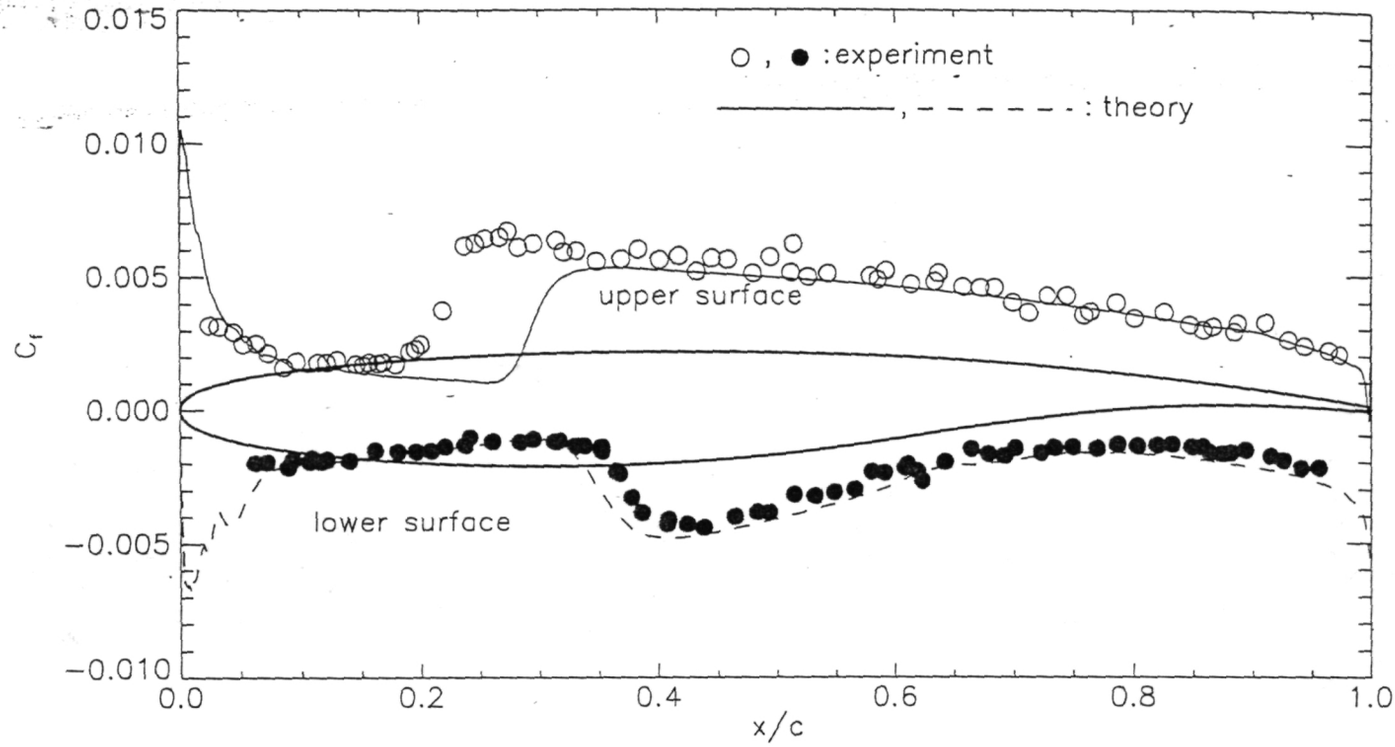

6(a) Re=$2x10^6$, α=0 deg.

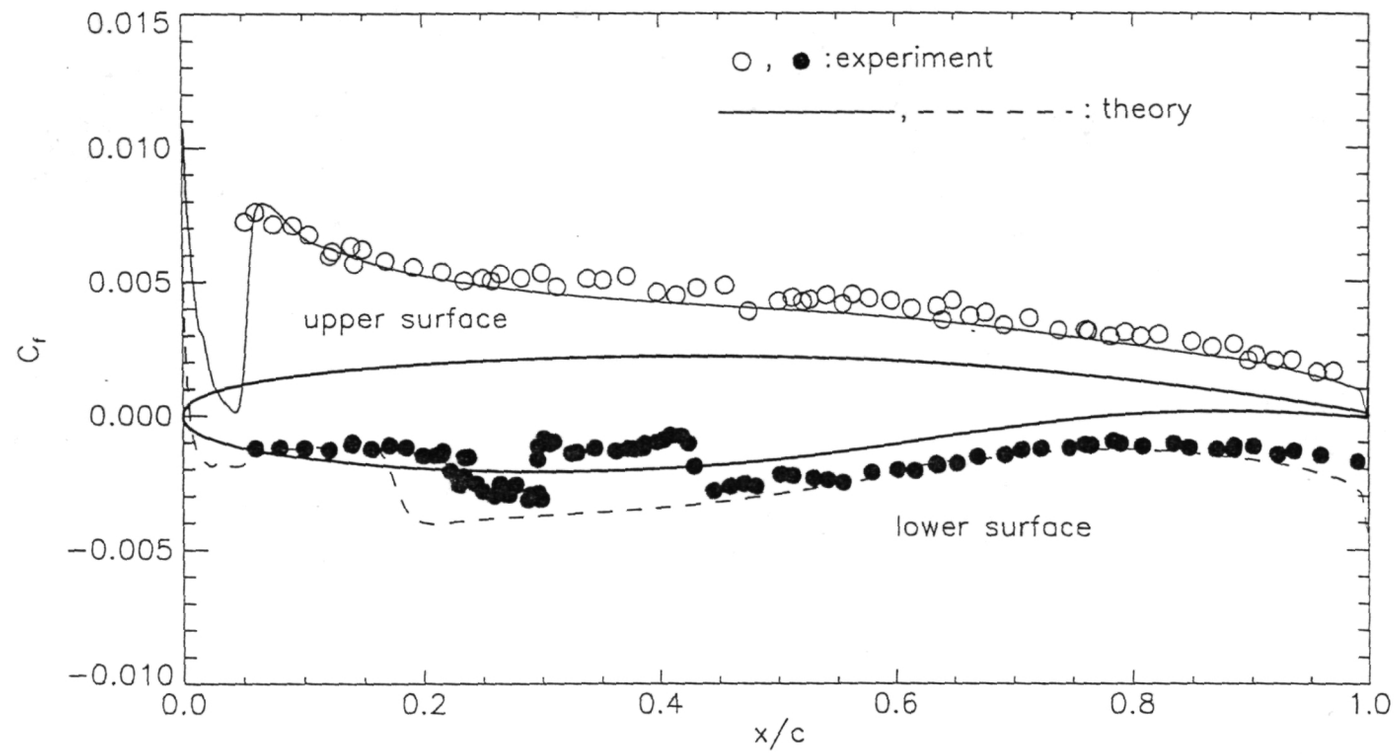

6(b) Re=$6x10^6$, α=4 deg.

Figure 6. Experimental and computational comparison of skin-friction coefficients on MBB VA-2 wing, M_∞=0.2

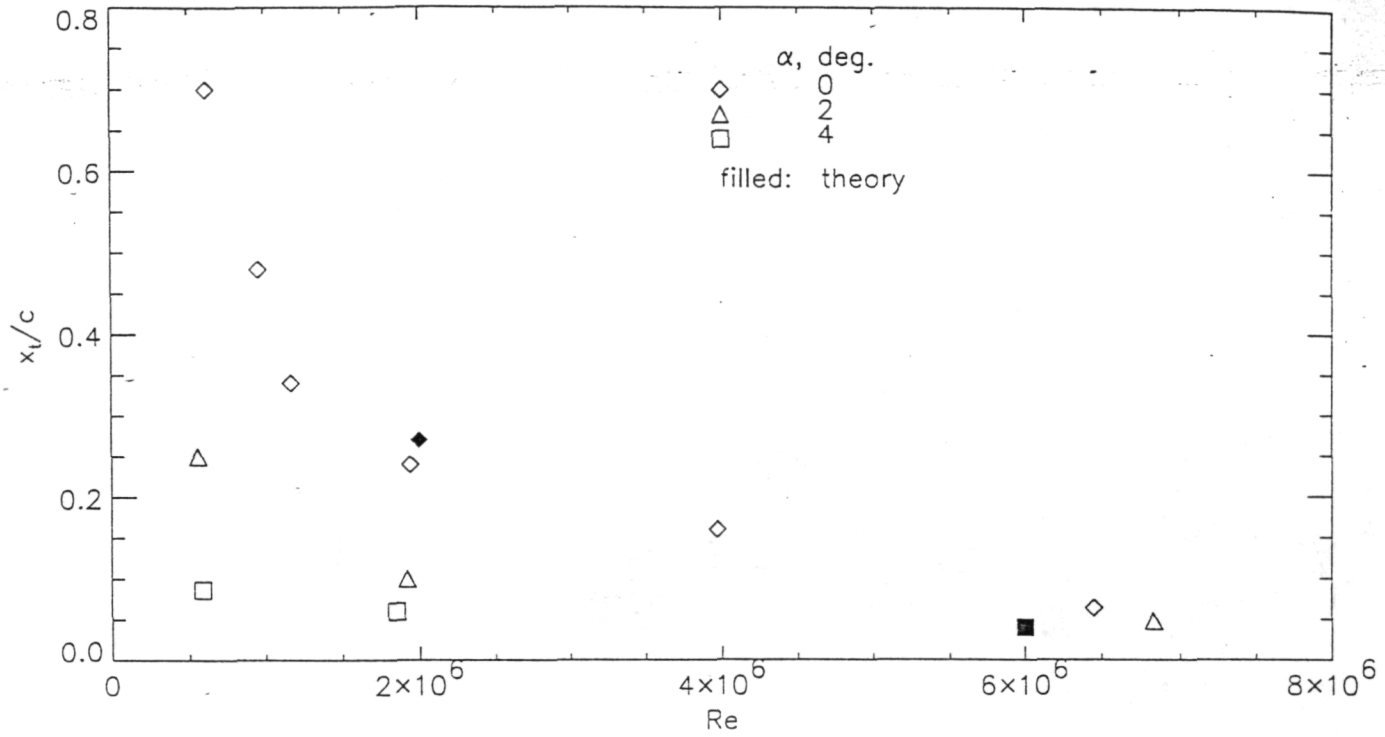

7(a) Upper surface

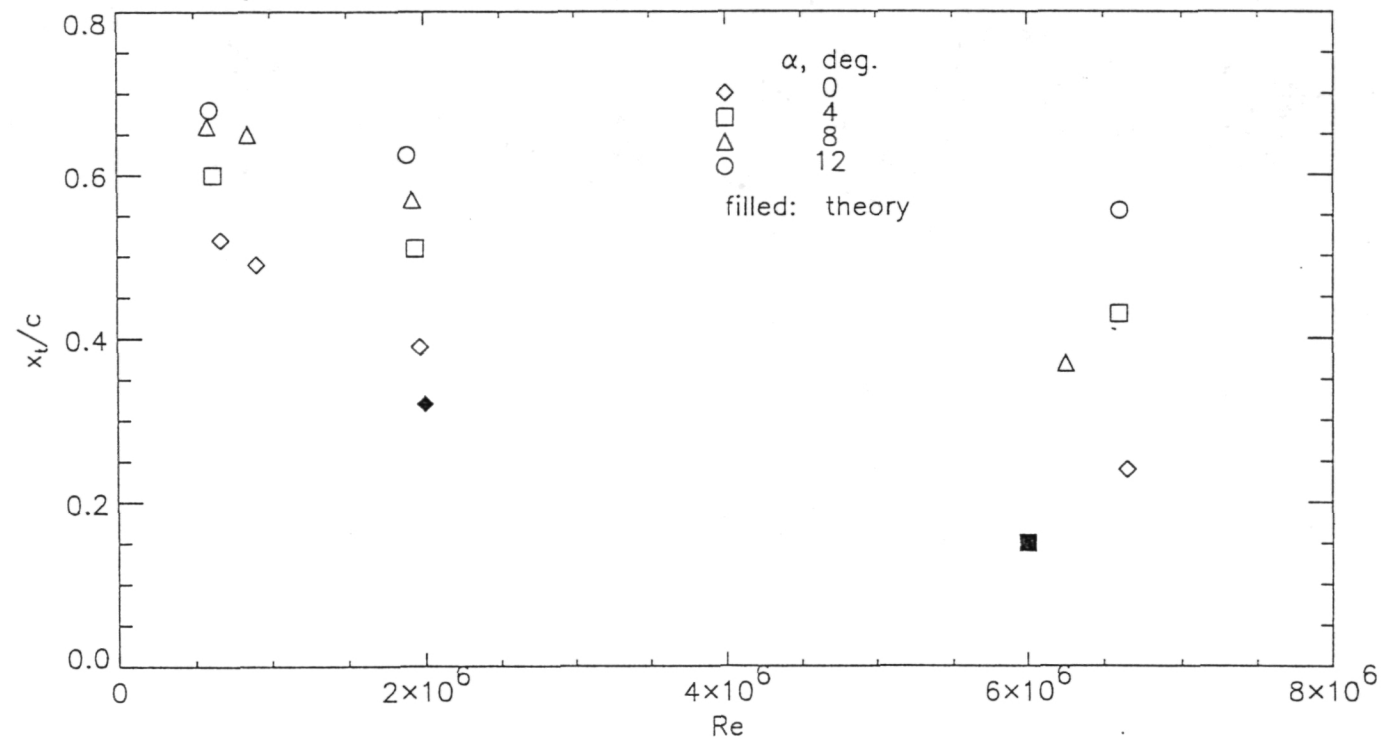

7(b) Lower surface

Figure 7. Measured and computed transition locations on MBB VA-2 wing, M_∞=0.2